Bio-inspired hybrid BFOA-PSO algorithm based reactive power controller in a standalone wind-diesel power system

Raju Wagle[1], Pawan Sharma[2,*†], Charu Sharma[3], Terje Gjengedal[4], and Chittaranjan Pradhan[5]

[1, 2, 3,4,5]*Department of Electrical Engineering, UiT The Arctic University of Norway, Narvik Campus, Norway*

SUMMARY

With an increase in the penetration of renewable energy sources such as wind into the power systems, the operation, and control of voltage/reactive power have become more complicated and challenging than ever. As a result, the reactive power imbalance between reactive power generation and demand instigates a reduction in system voltage stability. To deal with the aforesaid scenarios, automatic voltage regulator (AVR) and static synchronous compensator (STATCOM) are incorporated to curtail the voltage deviations in a standalone wind-diesel power system. In this paper, a hybrid bacterial foraging optimization algorithm-particle swarm optimization (hBFOA-PSO) algorithm is proposed for optimizing the PI-controller parameters of AVR and STATCOM to further improve the system voltage/reactive power performance. Additionally, H_∞-loop shaping technique is designed to analyze the performance indexes (i.e., robustness and stability) of the presented controller with the aim of handling the unstructured uncertainties from generation and loading situation. In order to present the efficiency of the proposed controllers, the performance of the hBFOA-PSO controller is compared with the performance of the BFOA, PSO and modified grey wolf optimization (MGWO) based PI-controllers for the same wind-diesel system. The dynamic responses of the wind-diesel system for different disturbance cases have been investigated in the MATLAB/SIMULINK@ environment.

Keywords:

Bacterial foraging optimization algorithm (BFOA), hBFOA-PSO, PSO, PI-controller, Wind-diesel standalone power system.

*Correspondence to: **Pawan Sharma**, *Department of Electrical Engineering, UiT The Arctic University of Norway, Narvik Campus, Norway.* †E-mail: *pawan.sharma@uit.no*

1. Introduction

1.1 Motivation and Incitement

With an increase in the penetration of renewable energy sources such as wind into the power systems, the operation, and control of voltage/reactive power have become more complicated and challenging than ever. As a result, the reactive power imbalance between reactive power generation and demand instigates a reduction in system voltage stability. To deal with the aforesaid scenarios, automatic voltage regulator (AVR) and static synchronous compensator (STATCOM) are incorporated to curtail the voltage deviations in a standalone wind-diesel power system. In this paper, a hybrid bacterial foraging optimization algorithm-particle swarm optimization (hBFOA-PSO) algorithm is proposed for optimizing the PI-controller parameters of AVR and STATCOM to further improve the system voltage/reactive power performance. Additionally, H∞-loop shaping technique is designed to analyze the performance indexes (i.e., robustness and stability) of the presented controller with the aim of handling the unstructured uncertainties from generation and loading situation. In order to present the efficiency of the proposed controllers, the performance of the hBFOA-PSO controller is compared with the performance of the BFOA, PSO and modified grey wolf optimization (MGWO) based PI-controllers for the same wind-diesel system. The dynamic responses of the wind-diesel system for different disturbance cases have been investigated in the MATLAB/SIMULINK@ environment.

1.2 Literature Review

During the power system operation, voltage deviation is usually a consequence of power mismatch due to unexpected disturbances, such as sudden load leaping/dropping or generator tripping, etc. In the previous literature, with the aim of augmenting the dynamic voltage/reactive power control performance, the researchers have recommended various

control approaches/devices (e.g., robust control, FACTS devices, etc.) and/or soft computing algorithms in the wind-based power systems [6-10]. The enhancement of voltage stability in a wind-diesel hybrid power system using STATCOM and PID-controller with a derivative filter is observed in [7]. The performance of AVR is observed in [8] to ensure stability, robustness, and minimum overshoot by using the optimization process. In [9], [10] the coordinated operation of STATCOM and AVR is demonstrated. From this study, it is analyzed that the combined operation of controllers contributes a superior voltage performance in terms of robustness and stabilizing effects. Dynamic reactive power control and adaptive voltage management for a hybrid microgrid consisting of wind and diesel generators using a unified power flow controller (UPFC) is studied in [11].

With respect to the robust control approach, H∞-controllers are more robust against variation in power demand and system uncertainties [12], [13]. In [12], H_∞-based multivariable robust control scheme is proposed for regulating the voltage of a standalone microgrid consisting of diesel, PV, super-capacitor. In [13], H_∞-shaping weighting function is used to synthesize the robustness of the controller. In [8], [14] the authors have recommended the H_∞-loop shaping method for designing robust controllers. Seeing the usefulness of the H_∞-controller, H_∞-loop shaping approach is implemented to obtain the objective function of the studied power system for computing/designing the PI-controller parameters.

In practice, proportional (P)/PI/proportional plus integral plus derivative (PID)-controllers are mostly used in the industries and power system. In this perspective, the researchers have proposed numerous controller design approaches and formulations to optimize the gains of the controllers to fit the dynamics of the power system [15]. The intelligent optimization techniques like a genetic algorithm (GA) [16], BFOA [17], fuzzy-GWO [18], fuzzy-bat algorithm [9], Jaya algorithm [19], etc., have been developed and applied to solve different

optimization engineering problems such as tune/optimize the system/controller parameters. A comparative study of various soft computing techniques for reactive power compensation for the hybrid power systems is reported in [15]. In [16], the authors have implemented the genetic algorithm (GA) to adjust the PI-controller parameters of the SVC and AVR for reactive power control. Furthermore, a co-ordinate power management strategy between SVC, AVR, and wind-diesel based power system for proper power balancing is projected. In [18], the PI-controller tuned fuzzy-GWO algorithm is presented in a wind-diesel based system for improving reactive power performance. A coordinated fuzzy-Bat algorithm is studied for obtaining the optimized parameters for generators and STATCOM in a two-area power with the aim of improving the system voltage performance [9]. In [17], an optimal controller is designed for reactive power control in an isolated wind-diesel based power system using BFOA and the effectiveness of the suggested controller is compared with GA and PSO. In [20], the anti-bee colony algorithm and the GWO algorithm separately for automatic reactive power control of isolated wind–diesel hybrid power system. In [21], the authors used MGWO to obtain the optimum parameters of optimal PID-fuzzy-PID controller for load frequency control analysis in a two-area interconnected power system.

Even though numerous intelligent algorithms have been recommended to accomplish the optimal values of the controller/system parameters, they have their own shortcomings [15]. Hence, with the aim of improving search performance (i.e., convergence rate and optimized value of controller), the authors have recommended different hybrid algorithms by integrating two intelligent algorithms for reactive power control [21]–[27]. In [24], the Seeker Optimization Algorithm (SOA) is combined with Takagi-Sugeno (TS)-fuzzy logic controller for controlling reactive power and terminal voltage. In [25], the authors have suggested GA and Adaptive Neuro-fuzzy Inference System (ANFIS) approaches to preserve the optimal performance of STATCOM to control the voltage transients. In regard to the hBFOA-PSO

algorithm, it is employed for solving the optimization multi-modal and high dimensional benchmark functions [23]. Furthermore, the hBFOA-PSO is used for tuning the PI-controller parameters of the automatic generation control (AGC) in an interconnected two-area power system for enhancing the dynamic load frequency control (LFC) performance [26]. In [27], designing of the PI-controller parameters of the static var compensator (SVC) is reported in a multi-machine system for power system stability enhancement. Since the hBFOA-PSO (i.e., consists of BFOA and PSO) algorithm has a better search ability while avoiding the false and premature convergence, the hBFOA-PSO algorithm is implemented in an isolated wind-diesel system for reactive power control, in this paper. The hBFOA-PSO algorithm instigates better search performance than the PSO [28], BFOA [29], and MGWO [20] algorithms.

1.3 Contribution and Paper Organization

In this paper, a maiden attempt has been taken to apply hBFOA-PSO algorithm in a standalone wind-diesel based power system for reactive power control and suppressing the voltage deviations during the system events such as the variations in power demand and wind speed.

The main contributions made by authors in this paper:

1) The robustness (i.e., performance index) of the proposed controller on voltage deviation owing to fluctuation in reactive power is formulated by using the H_{∞}-loop shaping approach.
2) The hBFOA-PSO algorithm is implemented for optimizing the PI-control parameters of STATCOM and AVR in wind-diesel based power system for enhancing the system voltage/reactive power performances.
3) The efficacy of the hBFOA-PSO algorithm over BFOA, PSO, and MGWO based algorithms for reactive power control is verified in the same wind-diesel system considering different case studies.

The paper is structured as follows: The detailed mathematical modeling of the standalone wind-diesel based power system is presented in *Section-2* whereas the H_∞-controller design approach is illustrated in *Section-3*. In *Section-4*, an overview of the bio-inspired hBFOA-PSO algorithm is reported. Simulation results and discussions are observed in *Section-5*. Finally, the conclusion of the proposed control technique is provided in *Section-6*.

2. Modeling of the Standalone Wind-Diesel system

2.1 Wind Diesel System

In general, an induction generator (IG) is used as a wind energy conversion system (WECS) in wind power and the synchronous generator is used in diesel engines set for power generation. Despite several advantages of IG, the consumption of magnetization current for the excitation system results in poor performance in terms of lower voltage regulation, energy efficiency, and power factor [4]. In this context, a permanent magnet induction generator (PMIG) contributes a better voltage regulator/efficiency and power factor comparably to IG in the power system operation and control [4–5]. Hence, in this work, PMIG based wind integrated diesel generator system is considered for a stable, flexible, and secure power system operation and control. The schematic diagram of the studied isolated wind-diesel based power system is presented in Fig. 1.

In general, the diesel-generator set delivers the reactive power, whereas the wind generator and load consume it which is presented as in Fig. 1 (the power flow direction is indicated by arrow mark). The STATCOM absorbs/supplies the required reactive power in accordance with the system requirements for power balancing between the generations (i.e., diesel generator and PMIG) and load.

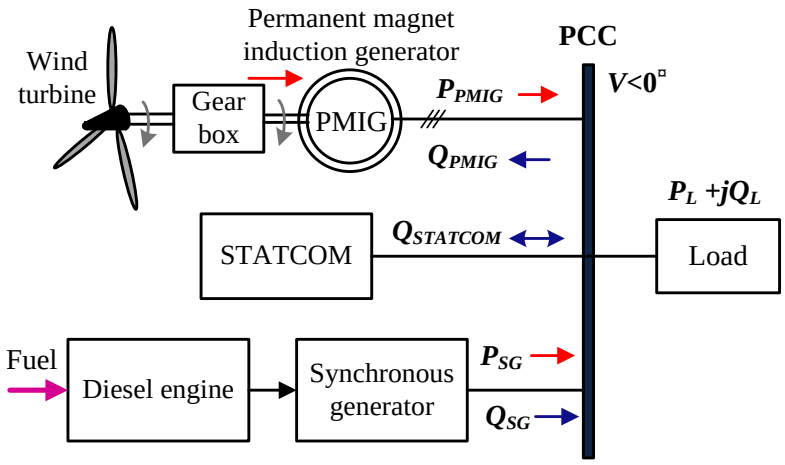

Fig. 1: Schematic of the standalone wind-diesel power system [29]

2.2 Linearized Model of system

linearized/small-signal models are convenient for designing the controller and analyzing the system reactive power/voltage performance of the power system with the variations/deviations in the system parameters, demand/generation, and so on [16], [17]. Hence, in this study, a small-signal/linearized model of wind-diesel based standalone power system with both STATCOM and AVR are considered as presented in Fig. 2. The presented small-signal/linearized model in Fig. 2 is a generalization functional diagram of the detailed power system model (Fig. 1). In this work, the variations in load reactive power (ΔQ_L), wind power (ΔP_{IW}) and voltage reference (ΔV_{ref}) signals are taken as the input variables and changes in system PCC voltage (ΔV) as the output variable in the linearized power system model. The modeling/design system parameters/data of the presented power system are specified in the *Appendix*.

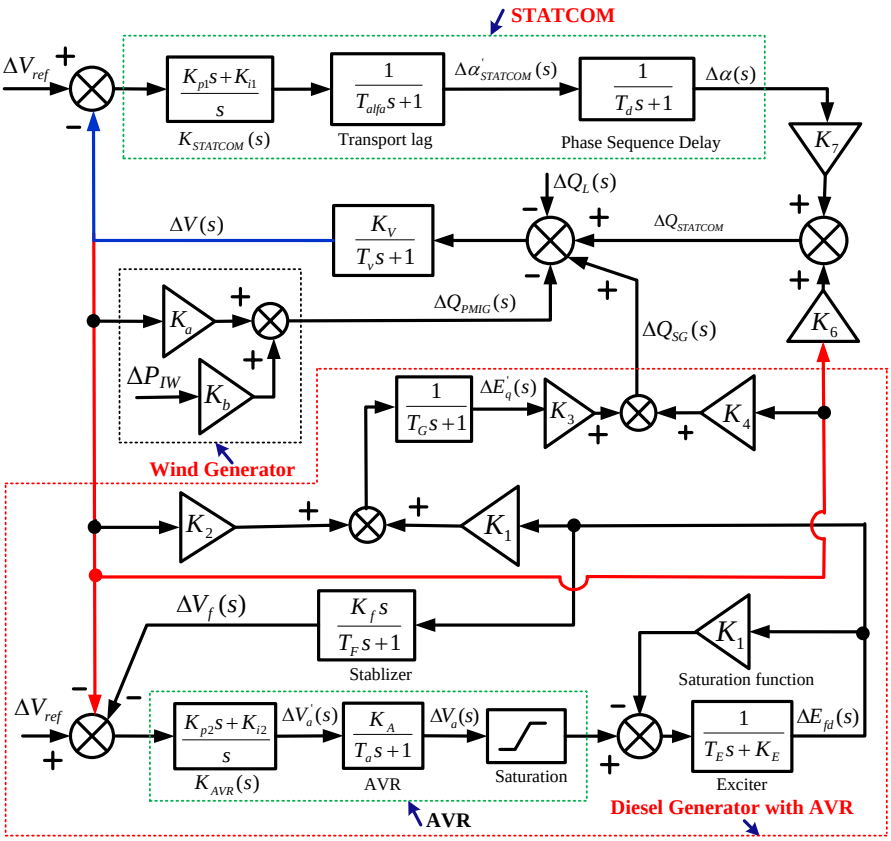

Fig. 2: Schematic of the linearized wind-diesel based power system

The reactive power and active power balancing equations for the above-mentioned power system (refer Fig. 1) under steady-state scenario are expressed as follows:

$$Q_{SG} + Q_{STATCOM} = Q_L + Q_{PMIG} \quad \text{and} \quad P_{PMIG} + P_{SG} = P_L \tag{1}$$

where, Q_{SG}, $Q_{STATCOM}$, Q_{PMIG} and Q_L are the reactive power of diesel generator, STATCOM, PMIG and load, correspondingly. P_{SG}, P_{PMIG} and P_L are the corresponding active power of diesel generator, PMIG and load, respectively.

By considering a small deviation (denoted by prefix Δ), the deviation in system voltage (ΔV) is derived w.r.t. the above-mentioned reactive powers as follows (refer Fig. 2) [27]

$$\Delta V(s) = \left(\frac{K_V}{1+sT_V}\right) * \left[\Delta Q_{SG}(s) + \Delta Q_{STATCOM}(s) - \Delta Q_L(s) - \Delta Q_{PMIG}(s)\right] \tag{2}$$

where, T_V is time constant, K_V is the system gain, ΔQ_{SG} is variation in output reactive power of the diesel based synchronous generator, $\Delta Q_{STATCOM}$ is the variation reactive power of STATCOM, ΔQ_L is the change reactive power load requirement, ΔQ_{PMIG} is the change reactive power of PMIG and ΔV is change system terminal voltage at PCC.

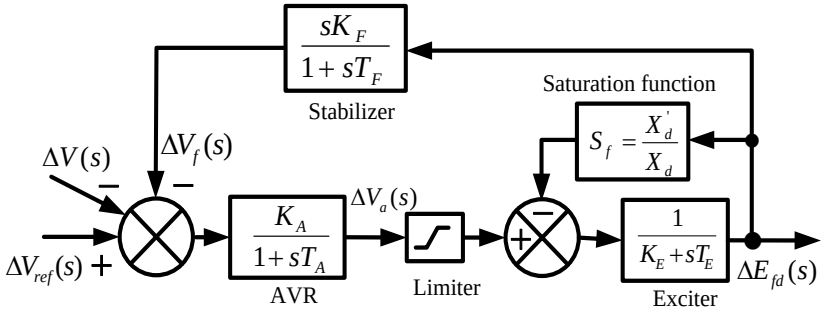

Fig. 3: Type-I IEEE excitation control system with $S_F = 0$ [28]

Furthermore, the small-signal model of Type-1 IEEE excitation control system of the diesel-generator with AVR is exhibited in Fig. 3. In Fig. 3, ΔV_{ref} is the reference voltage deviation. Neglecting the saturation function (i.e., S_F=0), the transfer functions of the excitation system are presented as follows [28]:

$$\Delta E_{fd}(s) = \frac{1}{K_E + sT_E}\Delta V_a(s) \tag{3}$$

with $\Delta V_a(s) = \frac{K_A}{1+sT_A}\left(\Delta V(s) - \frac{K_F}{T_F}\Delta E_{fd}(s) + \Delta V_f(s)\right)$ and $\Delta V_f(s) = \frac{K_F}{T_F}.\frac{1}{1+sT_F}\Delta E_{fd}(s)$

where, ΔE_{fd} is small change in excitation voltage, K_F is stabilizer time constant, K_E is excitation gain constant, T_E is exciter time constant, K_A is voltage regulator gain constant, T_A and T_F are time constant of voltage regulator and stabilizer, respectively.

Now, the devaition in armature voltage $\{\Delta E'_q(s)\}$ and reactive of the diesel powered synchronous generator $\{\Delta Q_{SG}(s)\}$ under transient condition is obtained in terms of the change in flux linkage (ΔE_{fd}) and voltage deviation (ΔV), which are written as follows [28]:

$$\Delta E'_q(s) = \frac{1}{(1+sT_G)}\left[K_1\Delta E_{fd}(s) + K_2\Delta V(s)\right] \tag{4}$$

$$\Delta Q_{SG}(s) = K_3\Delta E'_q(s) + K_4\Delta V(s) = \frac{1}{(1+sT_G)}\left[K_1\Delta E_{fd}(s) + K_2\Delta V(s)\right]K_3 + K_4\Delta V(s) \tag{5}$$

where, $K_1 = X'_d / X_d$; $K_2 = \left[\left(X_d - X'_d\right)\cos\delta\right] / X'_d$, $T_G = T'_{do}\ X'_d / X_d$, $K_3 = V\cos\delta / X'_d$ and $K_4 = \left[E'\cos\delta - 2V\right] / X'_d$, δ is power angle of synchronous generator, X'_d is direct-axis transient reactance of SG, T'_{do} is time constant of the direct-axis transient component and X_d is steady-state direct-axis reactance of SG.

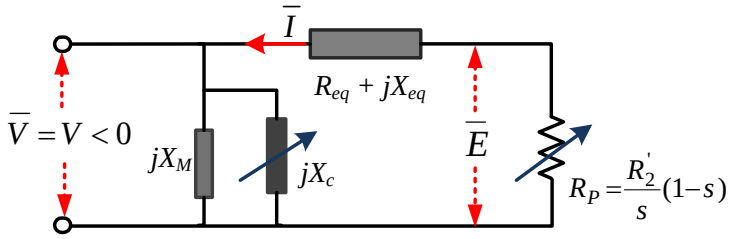

Fig. 4: Approximate equivalent model of PMIG [8]

Similarly, the variation in reactive power of the wind powered PMIG $\{\Delta Q_{PMIG}(s)\}$ is expressed as Equation-6. The equivalent circuit diagram of the PMIG is presented in Fig. 4. The detailed small-signal modeling of PMIG can be found in refs [6].

$$\Delta Q_{PMIG}(s) = K_a\Delta P_{IW}(s) + K_b\Delta V(s) \tag{6}$$

with $K_a = \dfrac{-2X_{eq}R_Y V^2}{(R_Y^2 + X_{eq}^2)\left\{2R_Y(P_{IW} - P_{coreloss}) + V^2\right\}}$, $K_b = \left[K_{c1} + \dfrac{V^2}{X_C}\left\{\dfrac{\left(3aV^2 + 2bV + c\right)}{\left(3X_C{}^3\right)} - \dfrac{2}{V}\right\}\right]$

$$K_{c1}=\frac{-2X_{eq}V}{R_Y^2+X_{eq}^2}\left[1+\frac{2R_YR_PV^2}{(R_Y^2+X_{eq}^2)\left\{2R_Y(P_{IW}-P_{coreloss})+V^2\right\}}\right],\quad R_Y=R_P+R_{eq}\quad\text{and}\quad X_C=(aV^3+bV^2+cV+d)^{1/3}$$

where, R_{eq} is the equivalent resistance of PMIG, X_{eq} is the equivalent reactance of the PMIG, ΔP_{IW} is the variation in input wind power, R_2' and X_2' are the rotor resistance and reactance corresponding to the primary-side of the PMIG, X_M is the mutual magnetizing reactance, X_C is the capacitive reactance, s is the slip of the PMIG. The design variables: a, b, c, d are the coefficients of the capacitive reactance component in the PMIG. The value of a, b, c and d are -7.8681, 15.4268, -9.782, 1.8899, respectively [30].

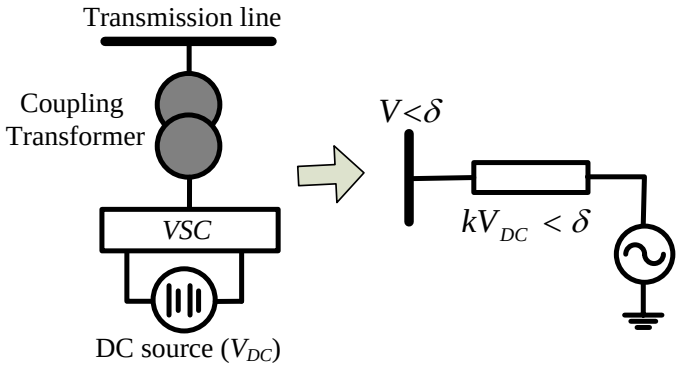

Fig. 5: STATCOM schematic diagram and equivalent diagram [8]

Additionally, the STATCOM is employed to produce/receive the required reactive power for maintaining a balanced three-phase sinusoidal voltage [6]. The schematic outline of STATCOM is presented in Fig. 5 which is capable of maintaining a balanced three-phase sinusoidal voltage at the fundamental frequency with controllable voltage amplitude and phase angle. The detailed modeling and operation of thyristor-based STATCOM can be found in [6]. For a small-perturbation, the variation in reactive power of STATCOM $\{\Delta Q_{STATCOM}\}$ is computed as follows [6]:

$$\Delta Q_{STATCOM}(s) = K_6 \Delta V(s) + K_7 \Delta \alpha(s) \quad (7)$$

with $K_6 = -kV_{dc} B \cos\alpha$ and $K_7 = kV_{dc} VB\ Sin\alpha$

where, $\Delta\alpha$ is the change in thyristor firing angle, B is the susceptance of the coupling transformer, kV_{dc} is the magnitude of the fundamental component of the converter output voltage.

3. H_∞ – loop shaping controller Design

From earlier literature studies, it is noticed that the H_∞-controller is a powerful tool to design robust controllers in a nonlinear system with uncertainties in system parameters [32]. It is true that the robustness criteria of a controller are not only the parameter to measure the overall performance of the controllers. However, the system performance parameters like steady-state error, settling time and under/overshoot are the important factors to be considered while designing a controller. It is highlighted that fixed structure H_∞-loop shaping technique compensates all these control problems and the optimization problem is formulated to measure the effectiveness {i.e., performance index (γ)} of the designed controller [32]. In this study, STATCOM and AVR are equipped by PI-controller and the optimization problem (i.e., objective function) of control parameters are stated by fixed structure H_∞-loop shaping technique for analyzing the robustness of the suggested controller. Furthermore, with the intention of enhancing the reactive power profile of the power system, hybrid BFOA-PSO (hBFOA-PSO) is employed to set the PI-control gains of STACOM and AVR. The brief discussion of hBFOA-PSO is presented in *Section-4*.

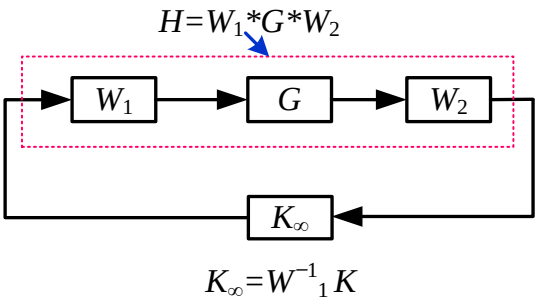

Fig. 6: H_∞ - shaped system controller [29]

The detailed design of the fixed structure robust H_∞-loop shaping controller can be found in [32]. The desired shape of open-loop frequency response in the H_∞-loop shaping is obtained by extending the nominal system/plant with pre-compensator and post-compensator as exhibited in Fig. 6. In Fig. 6, the shaped plant (H) is derived as $H=W_2GW_1$, where, W_1 and W_2 are the pre and post compensator, respectively. G is the transfer function of the plant (in this study, G is derived from the wind-diesel based power system which is demonstrated in Fig. 2) and K_∞ is the controller gain. In this study, the H_∞-norm (γ) is defined as the objective function (J) to tune the PI-controller coefficients for improving system performance as expressed in (8). A minimization control assignment is investigated to realize the minimum optimal solution (γ_{min}) of the cost/objective function (i.e., *Equation*-8). The key objective of the controller is to regulate the reactive power and minimize voltage deviations of the presented power system under load variations or system disturbances.

$$\text{Cost/objective function } (J) = \gamma = \left\| \begin{bmatrix} W_2 \\ W_1^{-1} K \end{bmatrix} (W_2 - H(s) W_1^{-1} K(s))^{-1} [W_1^{-1} \quad H(s)] \right\| \tag{8}$$

where, $K = \begin{bmatrix} K_{p1} + \frac{K_{I1}}{s} \\ K_{p2} + \frac{K_{I2}}{s} \end{bmatrix}$, $W_1 = \begin{bmatrix} 250\frac{s+20}{s+50} & 0 \\ 0 & 150\frac{s+30}{s+40} \end{bmatrix}$ and $W_2 = [\,\mathrm{I}\,]$

Subject to: $\begin{matrix} K_{p1,min} \le K_{p1} \le K_{p1,max} \\ K_{p2,min} \le K_{p2} \le K_{p2,max} \\ K_{I1,min} \le K_{I1} \le K_{I1,max} \\ K_{I2,min} \le K_{I2} \le K_{I2,max} \end{matrix} \Rightarrow \begin{matrix} 1 \le K_{p1} \le 575 \\ 1 \le K_{p2} \le 24000 \\ 0.0001 \le K_{I1} \le 100 \\ 0.0001 \le K_{I2} \le 100 \end{matrix}$

where, K_{p1} is the proportional gain and K_{I1} is the integral gain of STATCOM and K_{p2} and K_{I2} are the corresponding proportional gain and integral gain of AVR, respectively.

4. An overview of bio-inspired hBFOA-PSO algorithm

4.1. hBFOA-PSO algorithm

PSO is a stochastic search optimization method proposed by Dr. Eberhart and Dr. Kennedy in 1995, stimulated by the social manners of bird or fish schooling/swarming model [28]. In PSO, a direct search method is used to solve optimization problems where each particle adjusts their position in the search space with dynamic self-modified velocity. Established on this schooling/swarming model, the mathematical formulation is designed for upgrading the states (position, velocity) of the particles to obtain the best position/solution [28].

In addition, the BFOA is a swarm intelligent optimization presented by Dr. Passino. This algorithm is inspired by the foraging (methods of locating, handling, ingesting food) behavior of E. coli bacteria in locating their foods and is implemented for dealing with numerous optimization problems. The search mechanism of these bacteria comprises four fundamental steps such as swarming or tumbling, chemotaxis, reproduction, elimination, and dispersal [29].

With the purpose to enhance the search performance, the hBFOA-PSO algorithm is formulated by using the advantages of the above-mentioned algorithms (i.e., the ability of PSO to update its position dynamically on self-modified velocity, elimination and dispersal performance of BFOA) [23]. The hBFOA-PSO algorithm has numerous nested loops in order to improve search performance (i.e., achieve the optimal solution and faster convergence) [22]. The flowchart of the hBFOA-PSO is exhibited as Fig. 7. In this study, the collective performance/parameters of BFOA and PSO algorithms are considered to obtain the hBFOA-PSO algorithm for better-searching ability. In Fig. 7, *i*, *j*, *k* and *l* are the loop counters for the no. of bacteria (i.e., variables/populations), chemotaxis step, reproduction step and elimination

step, respectively. $J(i,j,k,l)$ is the solution/value of the cost function at the i^{th} variable for the k^{th} reproduction step and l^{th} elimination step during the j^{th} iteration. J_{last} is the previously obtained solution/value of the cost function at the i^{th} variable for the k^{th} reproduction stage and l^{th} elimination stage during the j^{th} iteration. To run (i.e., to obtain the optimal solution) the algorithms, the value of the BFOA, PSO, and hBFOA-PSO parameters are specified in *Table-I*. The details of the hBFOA-PSO algorithm can be found in [23].

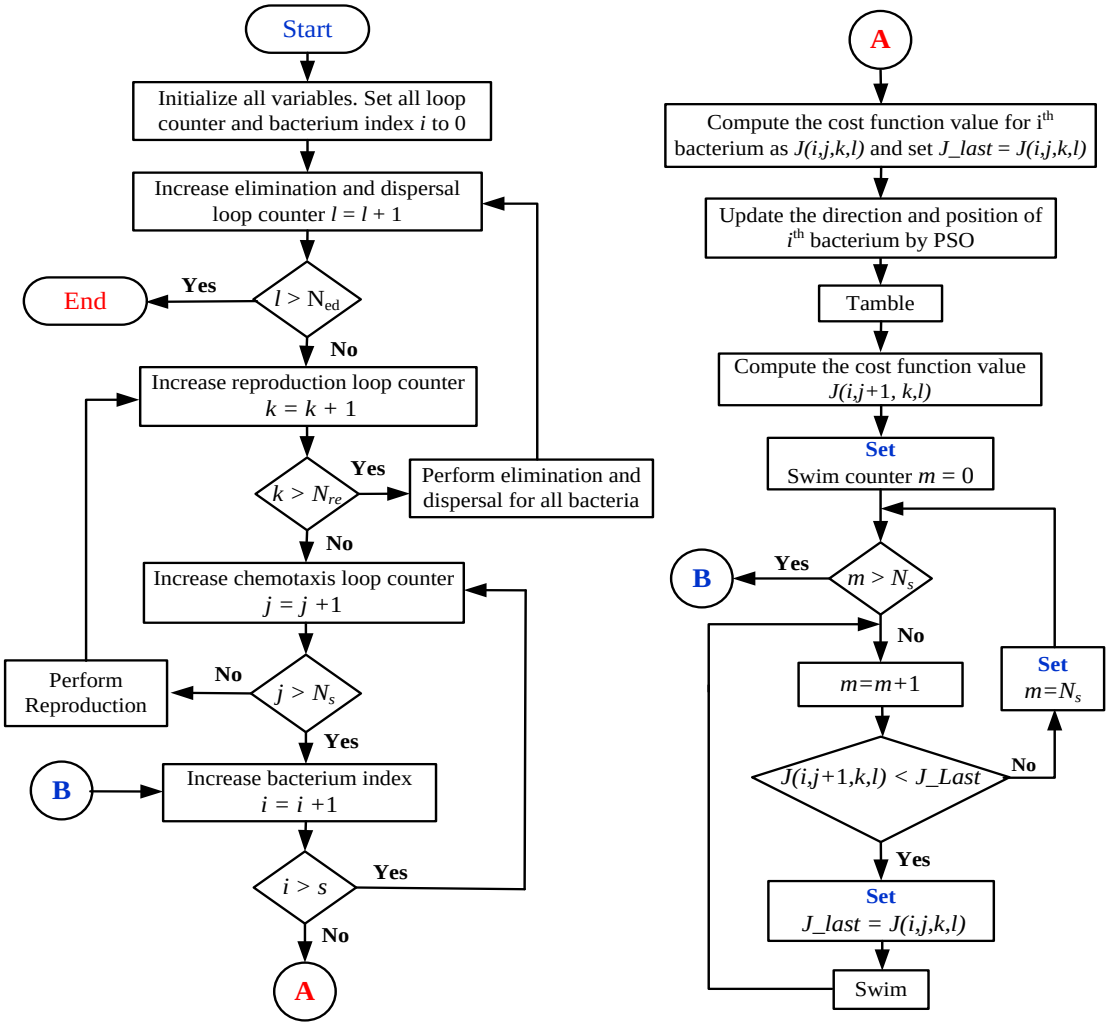

Fig. 7: Flowchart of the hBFOA-PSO [23]

Table-I: Values of control parameters of the hBFOA-PSO algorithm

Optimization algorithm	**Parameters**	**Value**
PSO [23]		
Cognitive parameter	c_1	0.5
Social parameter	c_2	0.5
Average value of momentum or inertia	w	0.5
BFOA [23]		
No. of bacteria or population size	s	50
Maximum no. of chemotactic steps or iteration	N_C	50
Length of a swim	N_S	4
No. of reproduction steps	N_{re}	2
No. of elimination-dispersal steps	N_{ed}	2
Probability that each bacteria to be eliminated	P_{ed}	0.25

4.2. Performance comparison of PSO, BFOA, MGWO and hBFOA-PSO

In this case study, the efficacy of the hBFOA-PSO algorithm over PSO [28], BFOA [29], and MGWO [20] have been verified on executing the objection function (J) of the presented isolated wind-diesel based power system (Fig. 2). GWO is a meta-heuristic search optimization algorithm that has been originally introduced by Dr. S. Mirjalili, *et al* in 2014 [33]. The algorithm is inspired by the hunting behavior of wolves in locating their foods and is used for solving various optimization problems. The details of the GWO algorithm can be obtained in [31]. In [20], [21], [33] the authors have demonstrated that the GWO algorithm has better search performance (e.g., faster computational convergence and getting the optimal solution) as compared with other evolutionary algorithms such as PSO, differential evolution (DE) and gravitational search algorithm (GSA), etc. Hence, in this work, the search performance of the hBFOA-PSO algorithm is equated with the recently developed MGWO algorithm which is presented in [21]. To obtain the optimal solution, the value of the control parameters of the MGWO is taken from [21].

The comparison of convergence curve BFOA, PSO, MGWO and hBFOA-PSO is displayed in Fig. 8 and it shows that the performance indices {i.e., achieve the minimal optimal solution of the cost function (J)} against the no. of iterations. From Fig. 8, it can be investigated that the hBFOA-PSO algorithm reasonably performs a better search performance in terms of optimal solution {i.e., performance index (γ_{min}) and faster convergence as compared to PSO, BFOA and MGWO algorithms. Moreover, it can be observed that all the algorithms achieve their minimal objective values (i.e., $J_{min}=\gamma_{min}$) for 50-iterations. Hence, for a fair comparison, 50-iterations have been chosen for attaining the minimum value of the cost function and tuning the PI-controller gains of STACOM and AVR, in this study. After solving the objective function (J) with considering power system parameters (referring *Appendix*) and the parameters of the algorithms (referring *Table-I*), the obtained minimal optimal value (γ_{min}) and the obtained PI-controller gains by each algorithm are presented below. The optimal proportional (K_p) and integral (K_i) gains of the PI-controllers obtained by PSO, BFOA, MGWO and the proposed hBFOA-PSO are listed in *Table-II*.

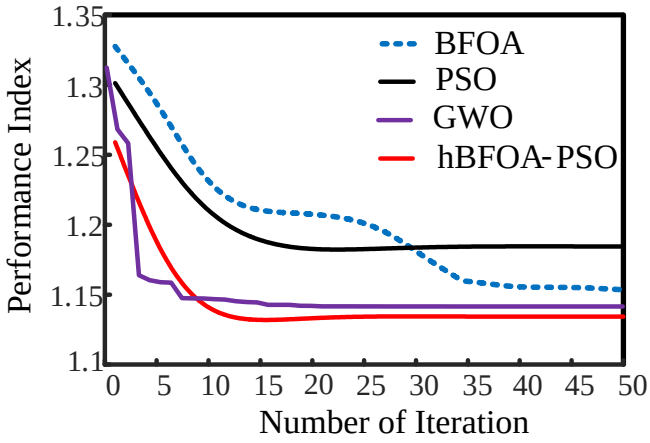

Fig. 8: Convergence curve of the objective function for BFOA, PSO and hBFOA-PSO

Table II: Optimal proportional and integral gains of the PI-controller

Optimization algorithm	STATCOM		AVR	
	K_{P1}	K_{I1}	K_{P2}	K_{I2}
PSO	154.5618	13610.5389	23.8067	36.6399
BFOA	112.4021	22420.1435	44.5765	49.2008
MGWO	123.0673	24000	33.1732	100
hBFOA-PSO	132.8909	23931.1152	13.0948	5.6002

5. Simulation Results and Discussions

The time-domain simulation studies are realized using the small-signal linearized model diagram (Fig. 2), the objective function (*Equation*-8) and the optimized PI-controller parameters of STATCOM and AVR (obtained by each algorithm in *Section-4.2*) by considering different case studies. All simulations and optimization algorithms are implemented in the MATLAB/Simulink power system simulation software. In this work, load reactive power perturbation (i.e., ΔQ_L) and change in wind power (i.e., ΔP_{IW}) are the input parameters and voltage deviation (i.e., ΔV) is the output parameter. The comparative Eigen values, performance index (γ_{min}), damping ratio (ξ) and settling time (t_s) of the voltage deviation and of the power system for each algorithm are presented in *Table-III.* Among four different algorithms, the hBFOA-PSO has a higher damping ratio (ξ=0.09851), faster settling time (0.0028s) and the lowest performance index (γ_{min}=1.1358) as compared to the BFOA, PSO and MGWO algorithms. Designing a robust controller with a proper damping ratio indicates that the controller response is sufficient enough to decay the oscillation after disturbance within the desired time frame. The higher the damping ratio slower is the oscillation and reducing the settling time of the system response [9]. From the findings, it can be examined that the hBFOA contributes to superior performance as compared to the BFOA PSO and MGWO search algorithms.

Table III: Comparative Eigen values, settling time of ΔV and performance index (γ_{min})

Different algorithms	Eigen values 1.0e+04 *	Settling time (t_s)	Damping ratio (ξ)	Performance index (γ_{min})
PSO	-6.7822 + 0i -0.0865 + 0i -0.1345 + 1.0746i -0.1345 - 1.0746i -0.0010 + 0.0155i -0.0010 - 0.0155i	0.0031s	0.05189	1.1863
BFOA	-6.7543 + 0i -0.0195 + 0i -0.1430 + 0.9945i -0.1430 - 0.9945i -0.0011 + 0.0122i -0.0011 - 0.0122i	0.0030s	0.0696	1.1648
MGWO	-6.7443 + 0i -0.0185 + 0i -0.1501 + 0.9361i -0.1501 - 0.9361i -0.0011 + 0.011i -0.0011 - 0.011i	0.0029	0.0871	1.1372
hBFOA-PSO	-6.7377 + 0i -0.0177 + 0i -0.1522 + 0.9154i -0.1522 - 0.9154i -0.0011 + 0.0105i -0.0011 - 0.0105i	**0.0028s**	**0.09851**	**1.1358**

Case I: ***Step perturbation in load reactive power*** **(ΔQ_L)**

For the above-mentioned optimization algorithms, the comparative response of deviation in bus voltage (ΔV) for a 1% step increase in load reactive power (ΔQ_L) at the time (t)=0s is displayed in Fig. 9. Furthermore, the corresponding dynamic deviations in reactive power of wind-based PMIG (ΔQ_{PMIG}), diesel-powered SG (ΔQ_{SG}), AVR (ΔQ_{AVR}) and STATCOM (ΔQ_{STACOM}) in the power system are presented in Fig. 9. From Fig. 9, it can be viewed that the hBFOA-PSO gives a superior dynamic performance (i.e., lower oscillations in voltage deviations with faster settling time, rise time and peak time) relatively than PSO, BFOA and MGWO. The dynamic statistical data/specifications of ΔV in terms of the settling time and over/undershoot, etc. are described in *Table-IV*. Moreover, the similar observations can be

obtained in the ΔQ_{PMIG}, ΔQ_{SG}, ΔQ_{AVR} and ΔQ_{STACOM} responses for PSO, BFOA, MGWO and hBFOA-PSO algorithms.

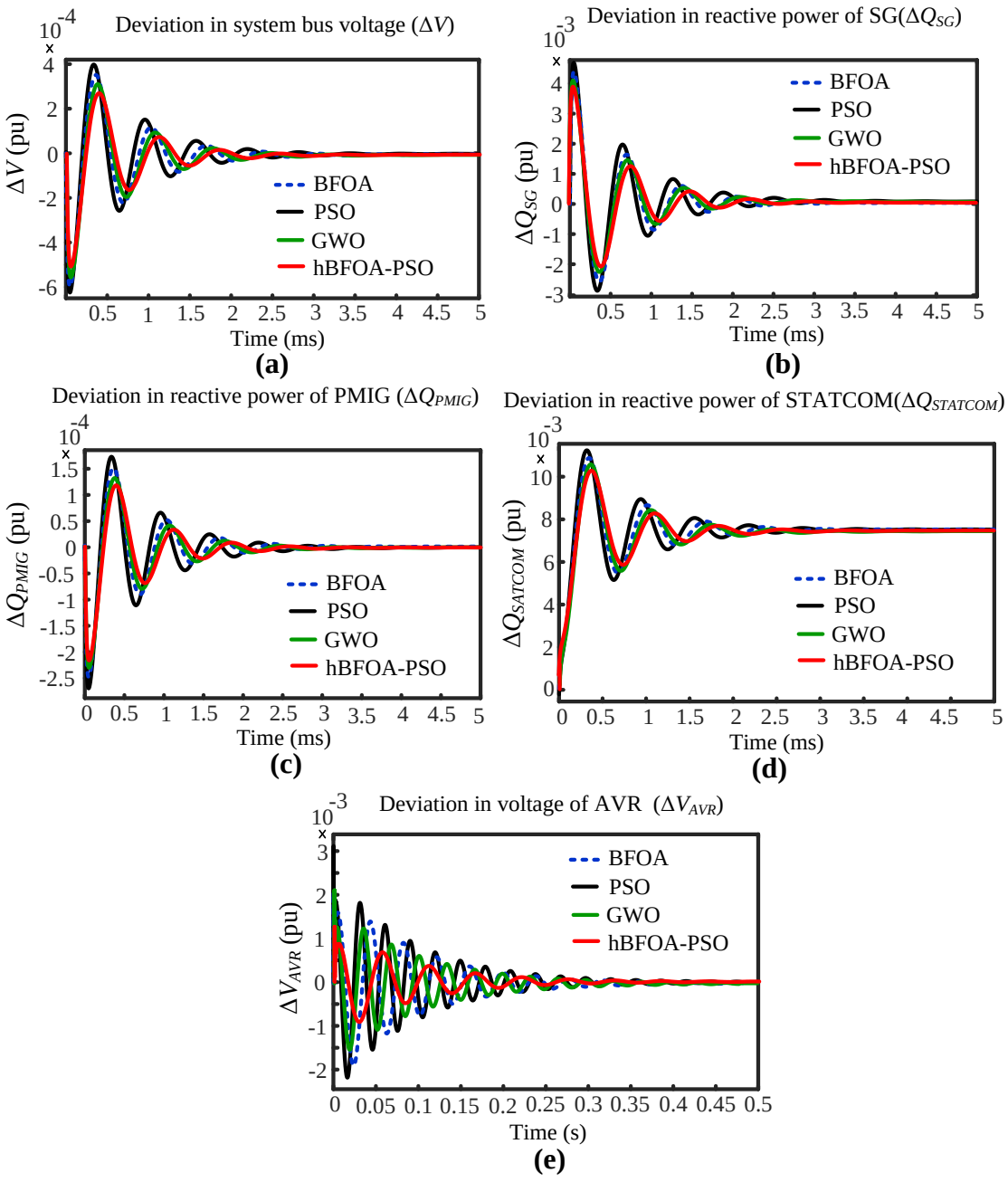

Fig. 7: Dynamic response for 1% increase in ΔQ_L

Table IV: Statistical data/specifications of ΔV for step information

Step info for change in system bus voltage (ΔV)								
Ref. Fig. 9(a)	Rise time (s)	Settling time (s)	Settling time min. (s)	Settling time max. (s)	Over shoot	Under shoot	Peak	Peak time (s)
PSO	4.81E-4	3.15E-3	3.015E-3	3.15E-3	4.12E-4	2.95E-4	4.1E-4	4.85E-04
BFOA	4.95E-4	3.05E-3	3.001E-3	3.05E-3	3.72E-4	2.72E-4	3.8E-4	4.95E-04
MGWO	4.98E-4	2.91E-3	2.901E-3	2.98E-3	3.65E-4	2.45E-4	3.6E-4	5.01E-04
hBFOA-PSO	5.01E-4	**2.85E-3**	**2.804E-3**	**2.86E-3**	**3.44E-4**	**2.15E-4**	**3.4E-4**	5.15E-04

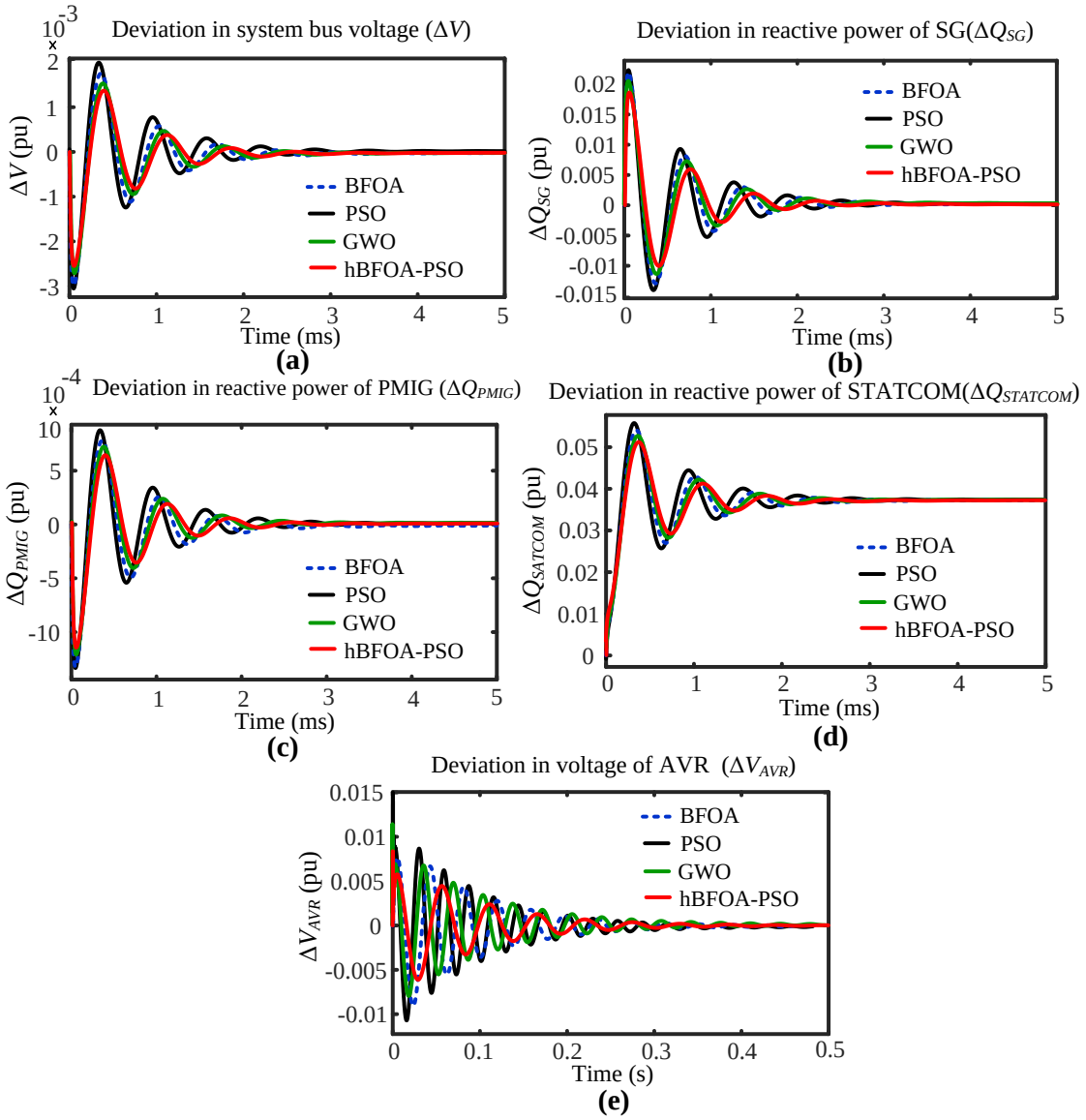

Fig. 10: Dynamic response for 5% increase in ΔQ_L

Similarly, the variations in system components such as ΔV, ΔQ_{PMIG}, ΔQ_{SG}, ΔQ_{AVR} and ΔQ_{STACOM}, for a 5% step increase in load reactive power (Q_L) at t=0s is shown in Fig. 10. From Fig. 10, it reveals that the hBFOA-PSO recovers the dynamics of the above-mentioned system components compared than PSO, BFOA and MGWO algorithms, after system disturbances. Furthermore, From Figs. 9 and 10, it can be observed that deviation is system bus voltage is higher for higher the variation in reactive power of the load.

Case II: Step perturbation in load reactive power (ΔQ_L) and input wind power (ΔP_{IW})

In this case, a step-perturbance in reactive power of load (i.e., ΔQ_L =1% increase) and input wind power (i.e., ΔP_{IW} =1% increase) occurs simultaneously at t=0s to present the efficacy of the hBFOA-PSO algorithm. For the above-mentioned input disturbances, the transient responses of ΔV, ΔQ_{PMIG}, ΔQ_{SG}, ΔQ_{AVR} and ΔQ_{STACOM} are displayed in Fig. 11. Fig. 11 represents that the results obtained by the hBFOA-PSO algorithm are improved than MGWO, BFOA and PSO algorithms.

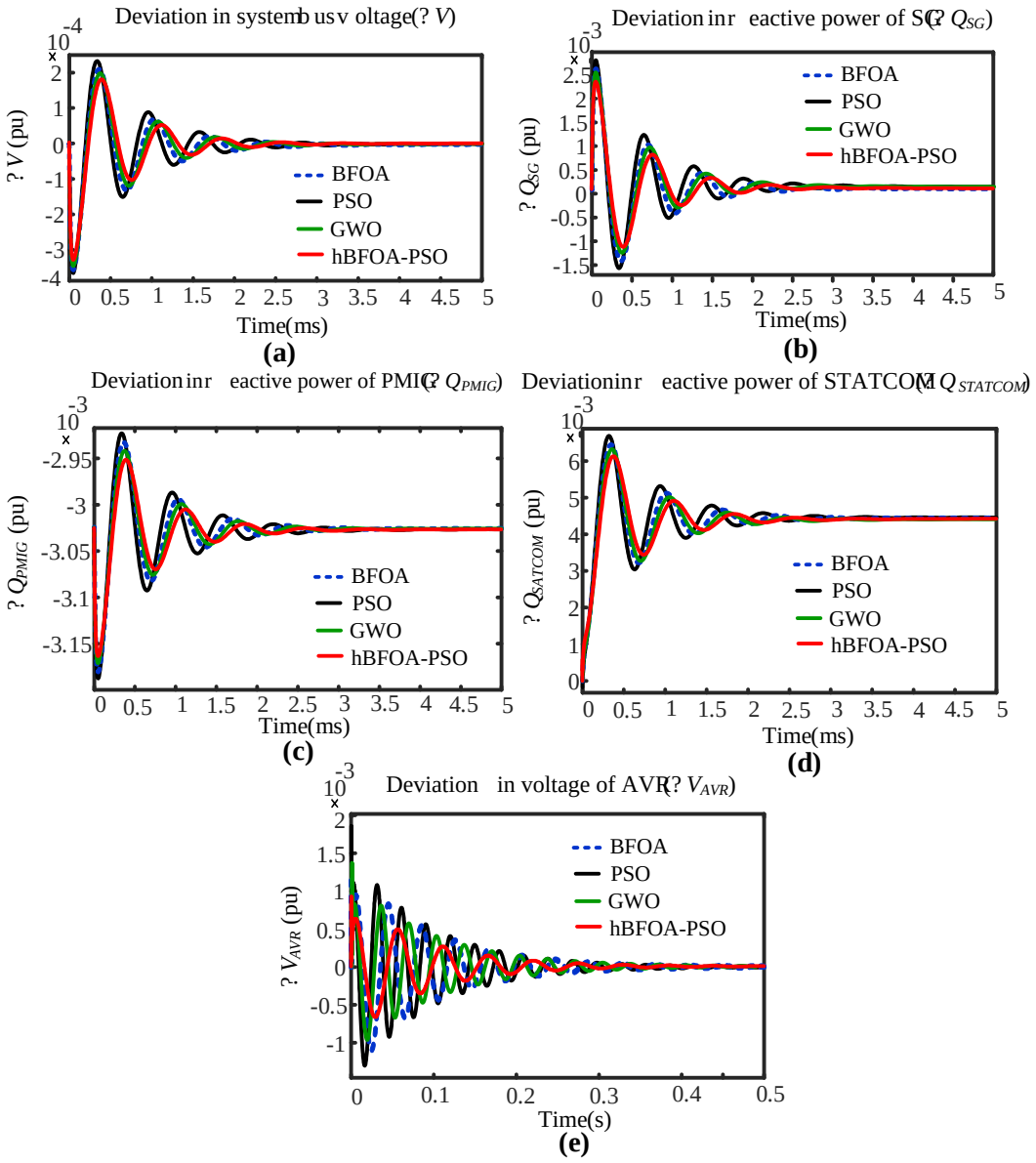

Fig. 11: Dynamic response of system for 1% increase in ΔQ_L with 1% increase in ΔP_{IW}

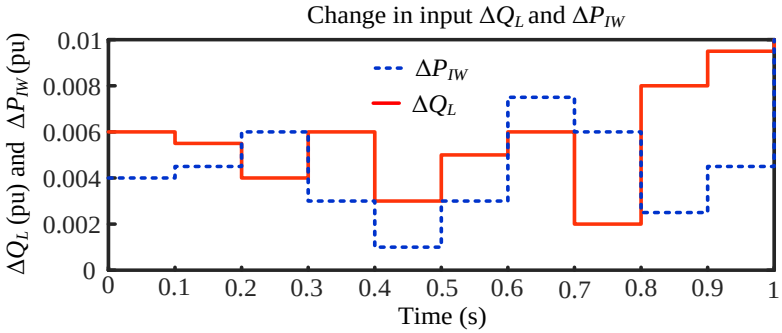

Fig. 12: Random changes in ΔQ_L and ΔP_{IW}

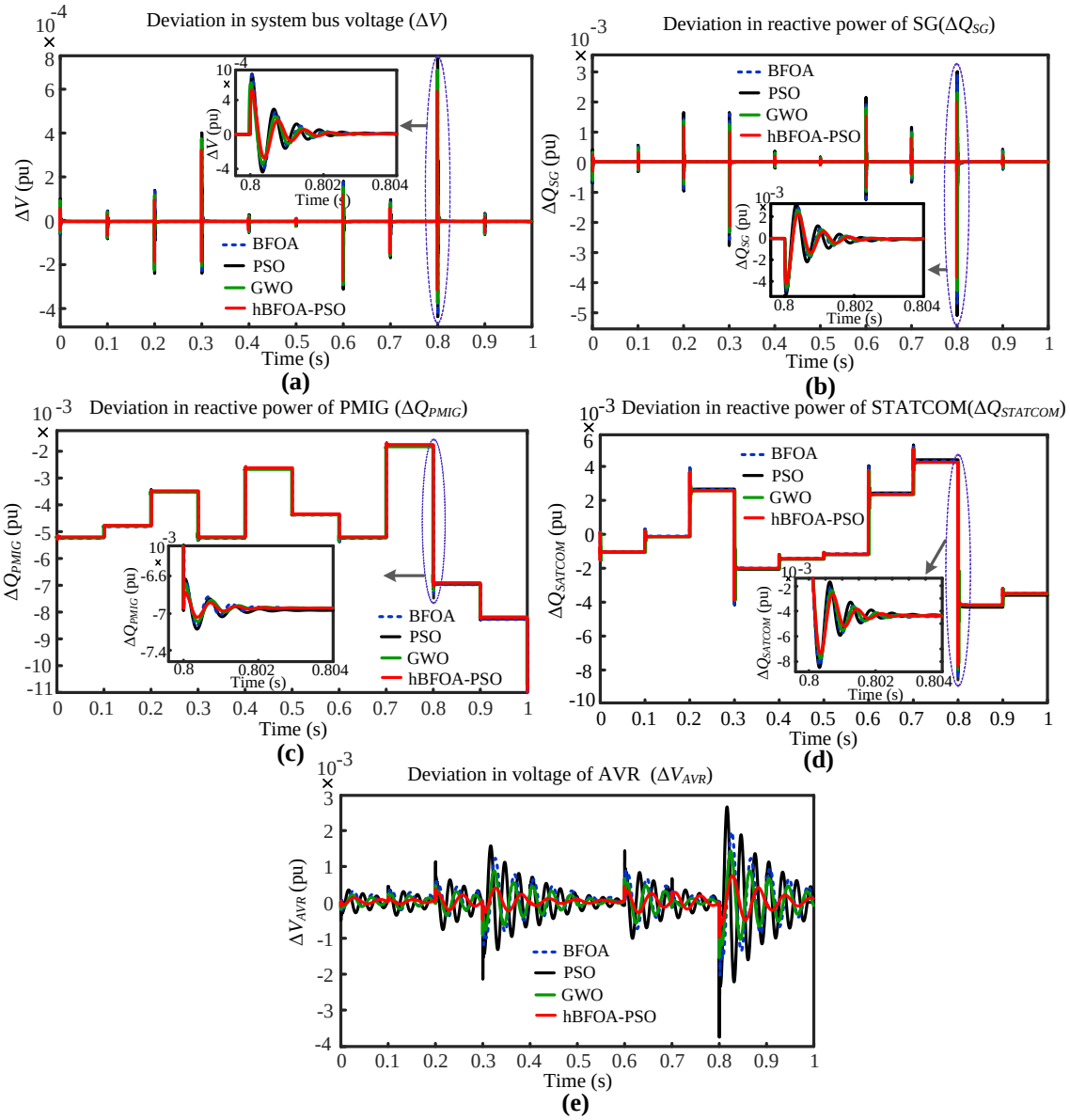

Fig. 13: Dynamic response for random step variation in ΔQ_L and ΔP_{IW}

In practice, the nature of load reactive power and wind power are random in nature which depends on the disturbance at the instant. Hence, in this case, random step-change in ΔQ_L and ΔP_{IW} are taken into consideration as in Fig. 12 to show the comparative performance of the hBFOA-PSO over PSO, BFOA, and MGWO algorithms. The dynamic responses of ΔV, ΔQ_{PMIG}, ΔQ_{SG}, ΔQ_{AVR} and ΔQ_{STACOM} are presented in Fig. 13, for each algorithm. From the findings, it can be noted that the hBFOA-PSO based reactive power system is more stable and superior than MGWO and when PSO, and BFOA algorithms execute individually. It can

be established that the hBFOA-PSO is effective for tuning the control gains of the PI-controllers in order to enhance the dynamic performance of the power system voltage/reactive power profile. Thus, this study is an effort to enable the wind-diesel based power system to solve the recent environmental and energy crisis issues and offers higher service reliability, increased energy efficiency, and energy independence.

6. Conclusions

In this paper, the dynamic voltage/reactive power performance of a standalone wind-diesel power system is analyzed by using the hBFOA-PSO optimization technique. The hBFOA-PSO algorithm is used for optimizing the gains of the PI-controllers of the AVR and STATCOM in order to improve the voltage stability of the power system and suppress the voltage/reactive power oscillations effectively during the system events such as the variations in power demand and wind speed. The time-domain simulation of the investigated power system model reveals that the hBFOA-PSO algorithm contributes better tuning capability and is relatively robust and stable in comparison to MGWO, BFOA, and PSO algorithms. The H_∞-loop shaping criteria is used for designing and analyzing the robustness (i.e., the performance index) of the proposed controller on voltage deviation owing to fluctuation in reactive power. The results indicate that the steady-state performance indices such as a minimum performance index (γ_{min}), and the transient performance indices like settling time, peak time, rise time, and over/undershoots in voltage deviation/reactive power responses are significantly improved for the suggested hBFOA-PSO of the power system.

Though a significant enhancement in the system stability in terms of faster dynamic compensation of voltage and reactive power is achieved with the proposed controller, the hBFOA-PSO may be applied to solve some other engineering optimization problems.

Modification of the proposed algorithm and propose of new hybrid optimization algorithms can be studied in future research work.

7. References

[1] S. R. Sinsel, R. L. Riemke, and V. H. Hoffmann, "Challenges and solution technologies for the integration of variable renewable energy sources—a review," *Renew. Energy*, vol. 145, pp. 2271–2285, 2020.

[2] S. Watson *et al.*, "Future emerging technologies in the wind power sector: A European perspective," *Renew. Sustain. Energy Rev.*, vol. 113, no. July, p. 109270, 2019.

[3] A. Gandhar, S. Gupta, M. Tiwari, and S. Gandhar, "A continuous mitigation of kVAR-voltage problem of hybrid isolated power system using UPFC," *J. Inf. Optim. Sci.*, vol. 41, no. 1, pp. 317–325, 2020.

[4] G. R. Biswal and B. Mohanty, "Voltage Control Method of Isolated Wind Power System," in *Advances in Electrical Control and Signal Systems*, 2020, pp. 361–371.

[5] R. Hunter and G. Elliot, *Wind-Diesel Systems*. 1994.

[6] B. Raouf, A. Akbarimajd, A. Dejamkhooy, and S. J. SeyedShenava, "Robust distributed control of reactive power in a hybrid wind-diesel power system with STATCOM," *Int. Trans. Electr. Energy Syst.*, vol. 29, no. 4, pp. 1–18, 2019.

[7] M. J. Blondin, P. Sicard, and P. M. Pardalos, "Controller Tuning Approach with robustness, stability and dynamic criteria for the original AVR System," *Math. Comput. Simul.*, vol. 163, pp. 168–182, 2019.

[8] P. Sharma, T. S. Bhatti, and K. S. S. Ramakrishna, "Study of an isolated wind–diesel hybrid power system with STATCOM by incorporating a new mathematical model of PMIG," *Eur. Trans. Electr. Power*, vol. 22, no. 3, pp. 351–363, 2012.

[9] P. Dahiya, P. Mukhija, and A. R. Saxena, "Design of sampled data and event-triggered load frequency controller for isolated hybrid power system," *Int. J. Electr. Power Energy Syst.*, vol. 100, no. May 2017, pp. 331–349, 2018.

[10] S. Gandhar, J. Ohri, and M. Singh, "Dynamic reactive power optimization of hybrid micro grid in islanded mode using fuzzy tuned UPFC," *J. Inf. Optim. Sci.*, vol. 41, no. 1, pp. 305–315, 2020.

[11] P. K. Guchhait and A. Banerjee, “Stability enhancement of wind energy integrated hybrid system with the help of static synchronous compensator and symbiosis organisms search algorithm,” *Prot. Control Mod. Power Syst.*, vol. 5, no. 1, 2020.

[12] M. Ramirez-gonzalez, R. Castellanos-bustamante, j guillermo Calderon-guizar, and M. Om P, “Coordinated design of fuzzy supplementary controllers for generator and STATCOM voltage regulators using bat algorithm optimization,” *Int. Trans. Electr. Energy Syst.*, no. February, pp. 1847–1862, 2016.

[13] L. C. Saikia and R. Rabongshi, “Performance of coordinated interline power flow controller and power system stabilizer in combined multiarea restructured ALFC and AVR system,” *Int. Trans. Electr. Energy Syst.*, no. October 2018, pp. 1–22, 2019.

[14] Q. L. Lam and D. Riu, “Voltage Regulation in Stand Alone Microgrid with storage units: A multi variable H-infinity control approach,” in *CIRED Workshop*, 2018, no. 0511, pp. 1–4.

[15] B. E. Sedhom, M. M. El-Saadawi, A. Y. Hatata, and E. E. Abd-Raboh, “A multistage H-infinity–based controller for adjusting voltage and frequency and improving power quality in islanded microgrids,” *Int. Trans. Electr. Energy Syst.*, vol. 30, no. 1, pp. 1–34, 2020.

[16] R. A. Davidson and S. Ushakumari, “H-Infinity Loop-Shaping Controller for Load Frequency Control of a Deregulated Power System,” *Procedia Technol.*, vol. 25, no. Raerest, pp. 775–784, 2016.

[17] P. K. Guchhait, A. Banerjee, and V. Mukherjee, “Comparative study using soft computing techniques for the reactive power compensation of a hybrid power system model,” *Ain Shams Eng. J.*, vol. 11, no. 1, pp. 87–98, 2020.

[18] S. Vachirasricirikul, I. Ngamroo, and S. Kaitwanidvilai, “Coordinated SVC and AVR for robust voltage control in a hybrid wind-diesel system,” *Energy Convers. Manag.*, vol. 51, no. 12, pp. 2383–2393, 2010.

[19] I. K. Aidoo, P. Sharma, and B. Hoff, “Optimal controllers designs for automatic reactive power control in an isolated wind-diesel hybrid power system,” *Int. J. Electr. Power Energy Syst.*, vol. 81, pp. 387–404, 2016.

[20] C. Pradhan and C. N. Bhende, “Online load frequency control in wind integrated power systems using modified Jaya optimization,” *Eng. Appl. Artif. Intell.*, vol. 77, no. December 2017, pp. 212–228, 2019.

[21] M. K. Debnath, T. Jena, and S. K. Sanyal, “Frequency control analysis with PID-fuzzy-

PID hybrid controller tuned by modified GWO technique," *Int. Trans. Electr. Energy Syst.*, vol. 29, no. 10, pp. 1–21, 2019.

[22] R. Wang, C. Tan, J. Xu, Z. Wang, J. Jin, and Y. Man, "Pressure control for a hydraulic cylinder based on a self-tuning PID controller optimized by a hybrid optimization algorithm," *Algorithms*, vol. 10, no. 1, 2017.

[23] A. Biswas, M. M. El-Saadawi, and A. Y. Hatata, "Synergy of PSO and bacterial foraging optimization- a comparative study on numerical benchmarks," in *Advances in Soft Computing*, vol. 4, no. AISC, 2007, pp. 255–263.

[24] A. Banerjee, V. Mukherjee, and S. P. Ghoshal, "Modeling and seeker optimization based simulation for intelligent reactive power control of an isolated hybrid power system," *Swarm Evol. Comput.*, vol. 13, pp. 85–100, 2013.

[25] N. K. Saxena and A. Kumar, "Reactive power control in decentralized hybrid power system with STATCOM using GA, ANN and ANFIS methods," *Int. J. Electr. Power Energy Syst.*, vol. 83, pp. 175–187, 2016.

[26] M. Shiraliyan, P. Sharma, and C. Sharma, "Automatic reactive power control of isolated wind–diesel hybrid power system using artificial bee colony and gray wolf optimization," *Int. J. Green Energy*, vol. 15, no. 14–15, pp. 889–904, 2018.

[27] P. Sharma and T. S. Bhatti, "Performance investigation of isolated wind-diesel hybrid power systems with WECS having PMIG," *IEEE Trans. Ind. Electron.*, vol. 60, no. 4, pp. 1630–1637, 2013.

[28] R. C. Bansal, T. S. Bhatti, and D. P. Kothari, "Automatic reactive power control of isolated wind-diesel hybrid power systems for variable wind speed/slip," *Electr. Power Components Syst.*, vol. 32, no. 9, pp. 901–912, 2004.

[29] D. C. McFarlane and K. Glover, *Robust Controller Design using Normalized Coprime Factor Plant Description*. Springer, 1990.

[30] R. Eberhart and J. Kennedy, "Particle swarm optimization," in *Proceedings of the IEEE international conference on neural networks*, 1995, vol. 4, pp. 1942–1948.

[31] K. M. Passino, "Biomimicry of bacterial foraging for distributed optimization and control," *IEEE Control Syst. Mag.*, vol. 22, no. 3, pp. 52–67, 2002.

[32] S. Mirjalili, S. M. Mirjalili, and A. Lewis, "Grey Wolf Optimizer," *Adv. Eng. Softw.*, vol. 69, pp. 46–61, 2014.

8. LIST OF SYMBOLS AND ABBREVIATIONS

8.1. Symbols

G	System open loop transfer function
H	System shaped plant transfer function
S	Slip of the PMIG
s	Frequency parameter in the frequency-domain
V	System terminal voltage at point of common coupling (PCC)
D_v	Load Voltage characteristic
E_M	Electromagnetic Energy in PMIG
K_A	Voltage regulator gain constant
K_E	Exciter gain
K_f	Stabilizer gain
K_{I1}	Integral gain of STATCOM
K_{I2}	Integral gain of AVR
K_{p1}	Proportional gain constant of STATCOM
K_{p2}	Proportional gain constant of AVR
K_v	System gain of AVR
K_α	Firing angle gain
η_{PMIG}	Efficiency of PMIG
P_{in}	Aerodynamic input power of PMIG
P_L	Real power load requirement
P_{PMIG}	Real power output of PMIG
P_{SG}	Real power output of synchronous generator
Q_L	Reactive power load requirement
Q_{PMIG}	Reactive power output of PMIG
Q_{SG}	Reactive power output of synchronous generator
$Q_{STATCOM}$	Reactive power of STATCOM
R_1	Stator resistance of PMIG
S_{PMIG}	Apparent power of PMIG
T_A	Voltage regulator time constant
T_d	Dead time of thyristor
T_E	Exciter time constant
T_F	Stabilizer time constant
T_v	System time constant

T_α	Delay time of thyristor
W_1	Weighted value of pre compensator
W_2	Weighted value of post compensator
X_1	Stator reactance of PMIG
X_D	Steady state direct axis reactance of synchronous generator
X_M	Magnetizing reactance of PMIG
α^o	Nominal firing angle of thyristor
Γ_k	*H*-infinity norm
γ_k	Performance index of
ΔE_{fd}	Small change in excitation voltage
ΔE_q	Small change in armature voltage
ΔM_S	Uncertaintity in nominal plant
ΔN_s	Uncertaintity in nominal plant
ΔV	Small change in terminal voltage
ΔV_a	Small change in AVR output voltage
ΔV_f	Small change in exciter feedback voltage
ΔV_{ref}	Small change in reference voltage
E'_{fd}	Small change in excitation voltage under transient
R'_2	Rotor resistance referred to primary side of PMIG
X'_2	Roror reactance referred to primary side of PMIG
T'_{d0}	Direct axis open circuit transient time constant
X'_d	Transisent state direct axis reactance of synchronous generator
α	Thyristor firing angle
δ	Power angle of Synchronous generator

8.2. Abbreviations

ANN	Artificial neural network
AVR	Automatic voltage regulator
BFOA	Bacteria Foraging optimization algorithm
BFOA-PSO	Bacteria Foraging optimization algorithm and Particle swarm optimization
FACTS	Flexible alternating current Transmission systems
GA	Genetic algorithm
hBFOA-PSO	Hybrid bacteria Foraging optimization algorithm and PSO

IG	Induction generator
PI	Proportional plus integral
PMIG	Permanent magnet induction generator
PSO	Particle swarm optimization
SG	Synchronous generator
STATCOM	Static synchronous compensator
SVC	Static VAR compensator (SVC)
WECS	Wind energy conversion System

Appendix:

Modelling/design parameters/data of the presented power system

System Parameters/data	Value	SI-unit
System Load/Capacity		
Wind capacity	150	KW
Diesel capacity	150	KW
Load Capacity	250	KW
Base Power	250	KVA
Synchronous Generator		
P_{SG}	0.4	Per unit (pu)
Q_{SG}	0.2	pu
E_q	1.1136	pu
Δ	21.05	^{0}
E_q'	0.9603	pu
V	1	pu
X_d	1	pu
X_d'	0.15	pu
T_G	5	Second (s)
Permanent Magnet Induction Generator		
P_{PMIG}	0.6	pu
Q_{PMIG}	0	pu
$R_1 + R_2'$	0.19	pu
$X_1 + X_2'$	0.59	pu
S	-4.0	%
Load		
P_L	1	pu
Q_L	0.75	pu
Power factor (lag)	0.8	
Reactive Power Data		
$Q_{STATCOM} + Q_{SG} = Q_{PMIG} + Q_L$	0.739	pu

Q_c	0.85	pu
A	2.443985	radian
IEEE Type-I Excitation System		
K_A	40	
T_A	0.05	Second (s)
K_F	0.5	
T_F	0.715	s
K_E	1	
S_F	0	s
T_E	0.55	s
STATCOM Data		
T_{alfa}	0.00025	s
T_d	0.00167	s